

Heat rectification, heat fluxes, and spectral matching

Javier Navarro

Department of Physical Chemistry, University of the Basque Country UPV/EHU, Apdo 644, Bilbao, Spain

Juan Gonzalo Muga

Department of Physical Chemistry, University of the Basque Country UPV/EHU, Apdo 644, Bilbao, Spain and EHU Quantum Center, University of the Basque Country UPV/EHU, 48940 Leioa, Spain

Marisa Pons

Department of Applied Physics, University of the Basque Country UPV/EHU, Bilbao, Spain and EHU Quantum Center, University of the Basque Country UPV/EHU, 48940 Leioa, Spain

(Dated: February 28, 2023)

Heat rectifiers would facilitate energy management operations such as cooling, or energy harvesting, but devices of practical interest are still missing. Understanding heat rectification at a fundamental level is key to help us find or design such devices. The match or mismatch of the phonon band spectrum of device segments for forward or reverse temperature bias of the thermal baths at device boundaries, was proposed as the mechanism behind rectification. However no explicit, theoretical relation derived from first principles had been found so far between heat fluxes and spectral matching. We study heat rectification in a minimalistic chain of two coupled ions. The fluxes and rectification can be calculated analytically. We propose a definition of the matching that sets an upper bound for the heat flux. In a regime where the device rectifies optimally, matching and flux ratios for forward and reverse configurations are found to be proportional. The results can be extended to a system of N particles in arbitrary traps with nearest-neighbor linear interactions.

I. INTRODUCTION

Heat rectification is a phenomenon in which the thermal energy that flows through a device between two reservoirs depends on the sign of their temperature bias [1–3]. Thus, an ideal heat rectifier or thermal diode would let heat flow only in one direction, for the “forward bias”, and act as an insulator for the “reverse bias” configuration with the bath temperatures exchanged. Such devices would serve for different energy management and thermal control operations, such as energy harvesting, refrigeration, or to implement thermal-based transistors, logic gates and logic circuits [2, 4, 5]. Proposed physical platforms for their applications go from the macro [1] to the microscale, for example in nanostructures [6], or trapped ions [7, 8]. The first experimental observations of this interesting phenomenon were due to Starr in 1936 [9]. Since then, much work has been done, but we are far from achieving useful devices [3, 10] in spite of the exploration of many different factors such as surface roughness/flatness at material contacts [1], thermal potential barriers [11], temperature dependence of thermal conductivity between different materials [12], nanostructured asymmetry (i.e. mass-loaded nanotubes, asymmetric geometries in nanostructures, nanostructured interfaces) [13], anharmonic lattices [14, 15], graded materials [16], long range interactions [17], localized impurities [18, 19], or quantum effects [3, 20]. For a more extensive list of references see the reviews [1–3, 6].

Theoretical work started with Terraneo *et al.* [14]. They showed thermal rectification in a segmented chain of coupled nonlinear oscillators in contact with two thermal baths at different temperatures. The heat rectifi-

cation was understood as a consequence of the match or mismatch of the phonon spectra of the different segments of the 1D chain when changing the temperature bias [2, 14, 21, 22]. The different dependences of the segments spectra with respect to temperature, implied conduction or isolation for the forward or the reverse bias. Li *et al.* [21], to describe the efficiency of the rectifier, analyzed the ratio of heat fluxes $|J/\tilde{J}|$ between the forward, J , and reverse, \tilde{J} , configurations. They found numerically, for their coupled nonlinear lattices model, a logarithmic relation between this ratio and the ratio of the degrees of overlap $|J/\tilde{J}|^\delta \sim \mathcal{S}/\tilde{\mathcal{S}}$ with \mathcal{S} and $\tilde{\mathcal{S}}$ being measures of the phonon-band overlap in the forward and reverse configurations. Yet this relation was not inferred from first principles. A theoretical connection between flux and matching, beyond the numerical findings, has been missing so far.

Nonlinear forces in the chain result in a temperature dependence of the phonon bands or power spectrum densities, possibly leading to rectification. However Pereira [23] pointed out that nonlinear forces are not a necessary condition for rectification, which only needs some structural asymmetry and a temperature dependence of some system parameters to occur. Indeed, the linear regime (i.e. harmonic interactions) is quite natural and realistic in some systems, such as trapped ions. Heat transport in trapped ion chains has been studied in several works [24–27]. Simón *et al.* [7, 8] proposed trapped ions as an experimentally feasible setting for heat rectification. They numerically demonstrated first heat rectification for linear chains of ions with graded trapping frequencies [7], and later in a minimalistic two-ion model [8]. For two trapped ions the asymmetry may be provided by differ-

ent species and the effective baths are implemented by Doppler cooling lasers that imply a temperature dependence of the couplings. The model is also quite interesting because the analytical treatment of several quantities, such as the flux, allows us to find optimal rectification conditions [8]. Moreover trapped ions constitute a well-developed and tested architecture for fundamental research, quantum information processing, and quantum technologies such as detectors or metrology. This architecture is in principle scalable in driven ion circuits (see, e.g., [28]). Controllable heat rectification in this context would be a useful asset for energy management in trapped-ion based technologies.

In this paper we find, for the two-ion linear ion chain, that a properly defined matching of the phononic spectra is an upper bound for the thermal flux. In Sect. II we provide an overview of the model. In Sect. III, we find a general relation between the thermal flux and the matching of the spectral densities. In Sect. IV matching and the flux are compared numerically. Finally, in Sect. V we present the conclusions and a generalization.

II. PHYSICAL MODEL

The minimalistic two-ion model describes two ions in individual traps subjected to Doppler cooling lasers [8] and a mutual Coulomb interaction, see Fig. 1. In the small oscillations regime, which is realistic for ions in multisegmented Paul traps, the model boils down mathematically to two harmonically coupled masses m_L and m_R (the subscripts refer to left and right and, when needed, will be described generically by the index $i = R, L$). Each mass is confined into a harmonic potential with spring constants k_L and k_R respectively, and in contact with thermal baths at different temperatures, T_L and T_R . The two masses are coupled through a spring with constant k [8]. x_L is the position of mass m_L and x_R is the position of mass m_R .

Without any coupling to the baths the system Hamiltonian is

$$H = \frac{p_L^2}{2m_L} + \frac{p_R^2}{2m_R} + V(x_L, x_R), \quad (1)$$

with $V(x_L, x_R) = [k_L(x_L - x_{eL})^2 + k_R(x_R - x_{eR})^2 + k(x_L - x_R - x_e)^2]/2$, where $\{x_i, p_i\}_{i=L,R}$ are the position and momentum of each mass, x_{eL} is the center of the left ion trap, x_{eR} is the center of the right ion trap, and x_e is the natural length of the linear coupling. Changing coordinates to the displacements from equilibrium positions of the system, $q_i = x_i - x_i^{eq}$, where x_i^{eq} are the solutions to $\partial_{x_i} V(x_L, x_R) = 0$, the Hamiltonian can be written as

$$H = \frac{p_L^2}{2m_L} + \frac{p_R^2}{2m_R} + \frac{k+k_L}{2} q_L^2 + \frac{k+k_R}{2} q_R^2 - kq_L q_R + V(x_L^{eq}, x_R^{eq}). \quad (2)$$

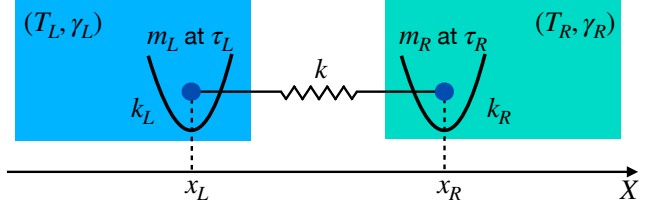


FIG. 1: Scheme of the model described in Sec. II. Each mass m_i is at temperature τ_i , ($i = L, R$ is the generic index for “left” or “right”), trapped by a harmonic potential, and connected to a thermal bath at a temperature T_i and friction coefficient γ_i . The masses interact by a harmonic potential with each other.

For later use let us define $V_i = (k + k_i)q_i^2/2$ and $V_{LR} = -kq_L q_R$. The constant term $V(x_L^{eq}, x_R^{eq})$ does not affect the evolution of the system so it can be ignored. The baths are modeled as Langevin baths so the friction coefficients γ_L, γ_R , and the Gaussian white-noise-like forces ξ_L and ξ_R are introduced into the equations of motion,

$$\begin{aligned} \dot{q}_L &= \frac{p_L}{m_L}, & \dot{q}_R &= \frac{p_R}{m_R}, \\ \dot{p}_L &= -(k + k_L)q_L + kq_R - \frac{\gamma_L}{m_L}p_L + \xi_L(t), & (3) \\ \dot{p}_R &= -(k + k_R)q_R + kq_L - \frac{\gamma_R}{m_R}p_R + \xi_R(t), \end{aligned}$$

where the following averages over noise realizations are assumed: $\langle \xi_i(t) \rangle = 0$, $\langle \xi_L(t)\xi_R(t') \rangle = 0$, $\langle \xi_L(t)\xi_L(t') \rangle = 2D_L\delta(t - t')$, and $\langle \xi_R(t)\xi_R(t') \rangle = 2D_R\delta(t - t')$. The diffusion coefficients D_L and D_R obey $D_L = \gamma_L k_B T_L$ and $D_R = \gamma_R k_B T_R$, where k_B is Boltzman’s constant.

A compact notation for the equations of motion is

$$\dot{\vec{r}}(t) = \mathbb{A}\vec{r}(t) + \mathbb{L}\vec{\xi}(t), \quad (4)$$

where $\vec{r}(t) \equiv (\vec{q}, \mathbb{M}^{-1}\vec{p})^\top = (q_L, q_R, \dot{q}_L, \dot{q}_R)^\top$ (the superscript \top means “transpose”), $\mathbb{M} = \text{diag}(m_L, m_R)$, and

$$\begin{aligned} \mathbb{A} &= \begin{pmatrix} \mathbb{0}_{2 \times 2} & \mathbb{1}_{2 \times 2} \\ -\mathbb{M}^{-1}\mathbb{K} & -\mathbb{M}^{-1}\mathbb{F} \end{pmatrix}, \\ \mathbb{L} &= \begin{pmatrix} \mathbb{0}_{2 \times 2}, \\ \mathbb{M}^{-1} \end{pmatrix}, & (5) \\ \mathbb{K} &= \begin{pmatrix} \frac{k+k_L}{2} & -k \\ -k & \frac{k+k_R}{2} \end{pmatrix}. \end{aligned}$$

Also $\vec{\xi}(t) = (\xi_L(t), \xi_R(t))^\top$ (note that \mathbb{L} is a 4×2 matrix), $\mathbb{F} = \text{diag}(\gamma_L, \gamma_R)$, $\mathbb{0}_{2 \times 2}$ is the 2×2 matrix with all the components 0, and $\mathbb{1}_{2 \times 2}$ is the 2×2 identity matrix.

The baths are implemented by optical molasses (Doppler cooling lasers) which set an effective temperature for each bath $T(= T_L, T_R)$, and an effective friction coefficient $\gamma(= \gamma_L, \gamma_R)$ which are controlled with the laser intensity I and frequency detuning δ with respect to the

selected internal atomic transition,

$$\begin{aligned}\gamma(I, \delta) &= -4\hbar \left(\frac{\delta + \omega_0}{c} \right)^2 \left(\frac{I}{I_0} \right) \frac{2\delta/\Gamma}{[1 + (2\delta/\Gamma)^2]^2}, \\ T(\delta) &= -\frac{\hbar\Gamma}{4k_B} \frac{1 + (2\delta/\Gamma)^2}{(2\delta/\Gamma)},\end{aligned}\quad (6)$$

where ω_0 is the (angular) frequency of the transition, c is the speed of light, I_0 is the saturation intensity, and Γ is the decay rate of the excited state. If Γ and I are fixed, γ depends on δ , and thus, indirectly, on the temperature T . In the two-ion model we deal in general with two different species which involve two different atomic transitions, so the laser wavelengths and the decay rates Γ depend on the species. Then, exchanging the temperatures by modifying the detunings, keeping the laser intensities constant, does not necessarily imply an exchange of the friction coefficients. Nevertheless, it is possible to adjust the laser intensities so that the friction coefficients get exchanged and this is the assumption in [8] and hereafter.

A. Covariance and spectral density

We are mostly interested in quantities such as the fluxes or particle temperatures in the steady state (s.s.) regime that is achieved after sufficiently long time. These quantities can be computed from the ‘‘marginal’’ correlation matrix $\mathbb{P}^{s.s.} = \langle \vec{r}(t) \vec{r}^\top(t) \rangle_{s.s.}$, which in the stationary regime does not depend on t .

Using the steady state condition, and Novikov’s theorem, the marginal covariance matrix in the steady state obeys [7, 29]

$$\mathbb{A} \mathbb{P}^{s.s.} + \mathbb{P}^{s.s.} \mathbb{A}^\top = -2\mathbb{L} \mathbb{D} \mathbb{L}^\top, \quad (7)$$

where $\mathbb{D} = \text{diag}(D_L, D_R)$. This equation may be used to solve for $\mathbb{P}^{s.s.}$. Alternatively the Fourier space may also be used. $\mathbb{P}^{s.s.} = \mathbb{C}^{s.s.}(0)$ is a particular case ($\tau = 0$) of the steady-state covariance matrix $\mathbb{C}^{s.s.}(\tau) = \langle \vec{r}(t) \vec{r}^\top(t + \tau) \rangle_{s.s.}$, which, according to the Wiener-Khinchin theorem [29]

$$\mathbb{C}^{s.s.}(\tau) = \langle \vec{r}(t) \vec{r}^\top(t + \tau) \rangle_{s.s.} = \mathcal{F}^{-1} [\mathbb{S}_{\vec{r}}(\omega)](\tau), \quad (8)$$

is the inverse Fourier transform of the the spectral density matrix

$$\mathbb{S}_{\vec{r}}(\omega) \equiv \left\langle \vec{R}(\omega) \vec{R}^\top(-\omega) \right\rangle, \quad (9)$$

where $\vec{R}(\omega) = (X_L, X_R, W_L, W_R)^\top$ is the Fourier transform (vector) of \vec{r} , namely

$$\mathbb{P}^{s.s.} = \mathbb{C}^{s.s.}(0) = \frac{1}{2\pi} \int_{-\infty}^{\infty} \mathbb{S}_{\vec{r}}(\omega) d\omega. \quad (10)$$

$\mathbb{S}_{\vec{r}}(\omega)$ may be computed as

$$\mathbb{S}_{\vec{r}}(\omega) = 2(\mathbb{A} - i\omega)^{-1} \mathbb{L} \mathbb{D} \mathbb{L}^\top (\mathbb{A} + i\omega)^{-\top}, \quad (11)$$

see [8, 29] for further details.

The diagonal matrix elements will be quite relevant for the analysis of the flux and matching. In particular the spectral densities $S_L \equiv \mathbb{S}_{3,3}(\omega) = \langle W_L(\omega) W_L(-\omega) \rangle$ for the left ion and $S_R \equiv \mathbb{S}_{4,4}(\omega) = \langle W_R(\omega) W_R(-\omega) \rangle$ for the right ion, where $W_i(\omega)$ is the Fourier transform of $\dot{q}_i(t)$, $i = L, R$, are (proportional to) power spectral densities of the kinetic energies since $m_i \langle \dot{q}_i \dot{q}_i \rangle / 2 = m_i \int S_i d\omega / (4\pi)$, see Eq. (10). The spectral densities S_L and S_R in terms of velocity transforms are related to the other diagonal elements $\mathbb{S}_{1,1}(\omega)$ and $\mathbb{S}_{2,2}(\omega)$, given in terms of displacement transforms, using the Fourier transform of the derivative,

$$\begin{aligned}S_L &= \omega^2 \langle X_L(\omega) X_L(-\omega) \rangle, \\ S_R &= \omega^2 \langle X_R(\omega) X_R(-\omega) \rangle,\end{aligned}\quad (12)$$

a property that we shall use later on to relate spectral overlap and flux.

B. Expressions for the flux

We will find now expressions for the flux, starting with the local energy for the left particle, defined as

$$H_L = \frac{1}{2m_L} p_L^2 + V_L(q_L) + \frac{1}{2} V_{LR}(q_L, q_R). \quad (13)$$

Differentiating with respect to time, we find the continuity equation

$$\begin{aligned}\dot{H}_L &= \frac{p_L \dot{p}_L}{m_L} + \frac{dV_L(q_L)}{dq_L} \dot{q}_L + \frac{1}{2} \frac{\partial V_{LR}(q_L, q_R)}{\partial q_L} \dot{q}_L \\ &\quad + \frac{1}{2} \frac{\partial V_{LR}(q_L, q_R)}{\partial q_R} \dot{q}_R.\end{aligned}\quad (14)$$

Using the equations of motion (4) into Eq. (14), and simplifying, we get

$$\begin{aligned}\dot{H}_L &= \frac{p_L}{m_L} F_{ext} - \frac{1}{2} \frac{\partial V_{LR}(q_L, q_R)}{\partial q_L} \dot{q}_L \\ &\quad + \frac{1}{2} \frac{\partial V_{LR}(q_L, q_R)}{\partial q_R} \dot{q}_R.\end{aligned}\quad (15)$$

where $F_{ext} = -\frac{\gamma_L}{m_L} p_L + \xi_L(t)$ includes the dissipative and the stochastic contributions. The first term in Eq. (15) due to the external force is the incoming flux of energy from the bath $J_{in} = p_L F_{ext} / m_L$. The second and third terms are the energy flux from particle L to particle R ,

$$J_{LR} = -\frac{1}{2} \frac{\partial V_{LR}(q_L, q_R)}{\partial q_L} \dot{q}_L + \frac{1}{2} \frac{\partial V_{LR}(q_L, q_R)}{\partial q_R} \dot{q}_R. \quad (16)$$

In the steady state $\langle \dot{H}_L \rangle = 0$ so the incoming flux and the flux of energy from the left particle to the right particle obey $-\langle J_{in} \rangle = \langle J_{LR} \rangle$. Then, the steady-state flux can be computed in two different ways. We will calculate $\langle J_{LR} \rangle$ first. Substituting $V_{LR} = -k q_L q_R$ in Eq. (16),

$$J_{LR} = \frac{1}{2} k (q_R \dot{q}_L - q_L \dot{q}_R). \quad (17)$$

Since we are interested in average values we define

$$J = -\langle J_{LR} \rangle = \frac{k}{2} [\langle q_L \dot{q}_R \rangle - \langle (q_R \dot{q}_L) \rangle]. \quad (18)$$

We apply the Wiener-Khinchin theorem to (18), to find the heat flux in the steady state,

$$\begin{aligned} J &= \frac{k}{4\pi} \int [\langle X_L(\omega) W_R(-\omega) \rangle - \langle X_R(\omega) W_L(-\omega) \rangle] d\omega \\ &= \frac{ki}{4\pi} \int \omega [\langle (X_R(\omega) X_L(-\omega)) \rangle - \langle X_L(\omega) X_R(-\omega) \rangle] d\omega \\ &= \frac{-k}{2\pi} \int \omega \text{Im} [\langle (X_R(\omega) X_L(-\omega)) \rangle] d\omega, \end{aligned} \quad (19)$$

where, in the second line we have used the Fourier transform property $W_i(\omega) = i\omega X_i(\omega)$. Since the positions are real, $X_i(\omega) = \bar{X}_i(-\omega)$.

An alternative expression for the flux may be computed from the incoming flux,

$$J_{in} = \frac{p_L}{m_L} \left[-\frac{\gamma_L}{m_L} p_L + \xi_L(t) \right]. \quad (20)$$

Averaging,

$$\langle J_{in} \rangle = -\frac{\langle p_L^2 \rangle}{m_L^2} \gamma_L + \frac{\langle p_L \xi_L(t) \rangle}{m_L}. \quad (21)$$

Since the left particle temperature is

$$\tau_L(t) = \frac{\langle p_L^2(t) \rangle}{m_L k_B}, \quad (22)$$

Eq. (21) and Novikov's theorem, see [7, 8] for a full calculation, give

$$\langle J_{in} \rangle = k_B \frac{\gamma_L}{m_L} (T_L - \tau_L). \quad (23)$$

For the steady state, $J = \langle J_{in} \rangle$ is equal to the alternative expression (19).

C. Rectification

We use as a measure of rectification the coefficient

$$R = \frac{||J| - |\tilde{J}||}{\max(|J|, |\tilde{J}|)}, \quad (24)$$

which is bounded between 0 and 1, $0 \leq R \leq 1$. Keep in mind that to exchange the baths from forward to reverse bias implies here to exchange the temperatures and the friction coefficients. A parametric exploration was done over the space formed by the parameters of the model $m_L, m_R, k, k_L, k_R, \gamma_L$ and γ_R to maximize R [8].

In [8] it was found that the region for maximal rectification for fixed masses could be described analytically, and in the weak dissipation regime

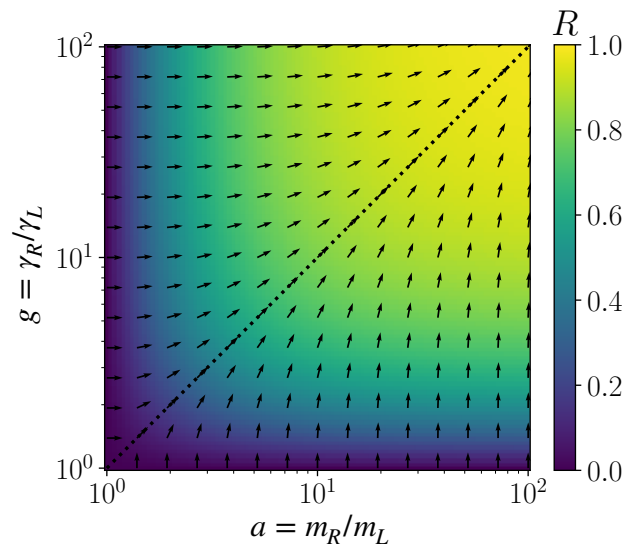


FIG. 2: Rectification, R , given by Eq. (26) as a function of the ratios a and g . The arrows give the gradient direction.

($\gamma_L/m_L \ll \sqrt{k/m_L}$, $\gamma_R/m_R \ll \sqrt{k/m_R}$) it is a straight line in the k_L, k_R plane, [8]

$$\frac{k + k_R}{m_R} = \frac{k + k_L}{m_L}. \quad (25)$$

On the maximum-rectification line (25) the rectification only depends on the mass and friction coefficient ratios a and g ,

$$R = \begin{cases} 1 - \frac{a+g}{1+ag} & \text{if } a > 1, g > 1 \text{ or } a < 1, g < 1 \\ 1 - \frac{1+ag}{a+g} & \text{if } a > 1, g < 1 \text{ or } a < 1, g > 1 \end{cases}, \quad (26)$$

where

$$a = m_R/m_L, \quad g = \gamma_R/\gamma_L. \quad (27)$$

Increasing a or g increases the asymmetry of the system and the rectification. From Eq. (26) we can represent R in terms of a and g , see Fig. 2. The fastest way of increasing R is following the diagonal dotted line $a = g$. For this reason, we shall mostly use the condition $a = g$ and sweep over the parameter $C \equiv a = g$. R grows with C towards one, but there are physical limitations to make these ratios arbitrarily large. In particular changing a is limited by the masses of the available ions. In numerical examples and calculations hereafter we shall always fulfill Eq. (25) and fix the following values: in the forward configuration $k = 1.17$ fN/m, $k_L = 1$ fN/m, $\gamma_L = 6.75 \times 10^{-22}$ kg/s, $m_L = 24.305$ a. u. (for Mg^+), whereas γ_R, m_R , and k_R are set to satisfy chosen values of g and a . Similarly k_R is set to satisfy Eq. (25). For the reverse configuration of bath temperatures we interchange the friction coefficients, $\tilde{\gamma}_L = \gamma_R, \tilde{\gamma}_R = \gamma_L$, but the masses and spring constants do not change with respect to the ones for the forward configuration. The

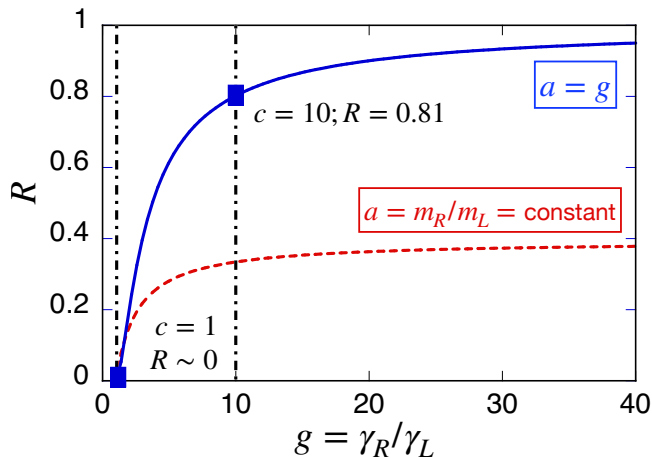


FIG. 3: Rectification for different values of $g = \gamma_R/\gamma_L$. The blue solid line gives the maximal rectification, which is found when for $a = g$, see Eq. (25). For the red dashed line the mass ratio is kept constant (corresponding to Mg^+ and Ca^+ ions). The blue squares correspond to the values of $C = 1$ (the two ions and the friction coefficients are equal, so $R \sim 0$), and $C = 10$, $R \sim 0.8$. The spectra for $C = 10$ are depicted in Fig. 4.

calculations of spectra using Eq. (11) depend on these values and on the bath temperatures (by the dependence on the temperature of the diffusion coefficients).

In Fig. 3 the rectification is depicted versus g when $a = g$ (blue solid line), and for a constant (red dashed line), which gives smaller rectification.

D. Spectral densities and rectification: Example

In [8], the spectra of the ions S_L and S_R for several sets of parameters exhibiting large and small rectification were studied. Indeed the system presented large rectification if, for a bath configuration, there is a good match between the phonon spectra of the ions and mismatch when the baths were exchanged.

Figure 4 shows the spectra $m_L S_L$ and $m_R S_R$ for $C = 10$, i.e., for high rectification, $R \sim 0.8$, see Fig. 3. For forward bias there is almost perfect matching between the spectral densities but a mismatch for the reverse configuration. This is a clear example of the qualitative relation between flux and spectral matching. In the following section we shall give this relation a more quantitative form.

III. RELATIONS BETWEEN SPECTRAL MATCHING AND HEAT FLUX

The matching M or overlap between the spectral densities has to be defined. A relevant definition would be one related to the flux, by a direct dependence, or by an inequality. We may expect as an ansatz a form depending

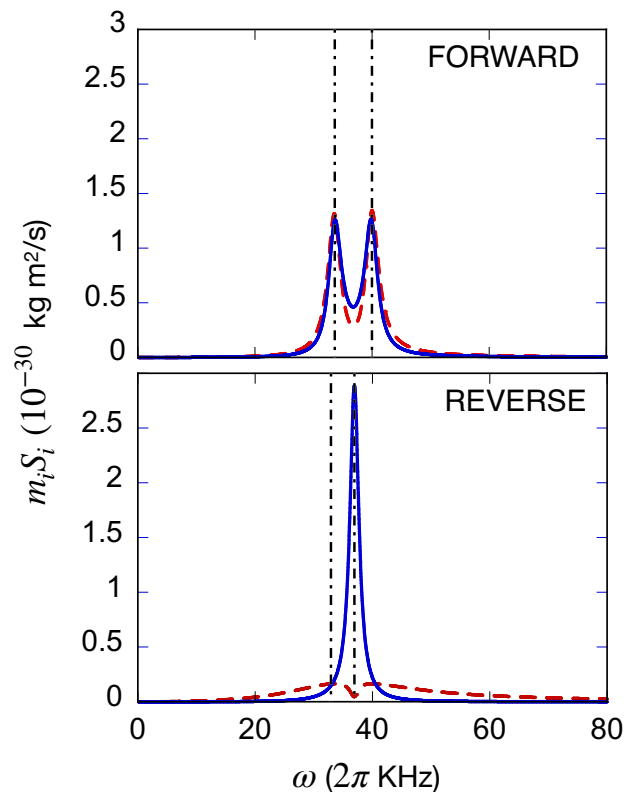


FIG. 4: Spectral densities for both ions multiplied by their masses, $m_L S_L$ (solid red line) and $m_R S_R$ (dashed blue line), vs. ω for $C = 10$ corresponding to forward and reverse configurations. $T_L = \tilde{T}_R = 2\text{mK}$, $T_R = \tilde{T}_L = 1\text{mK}$. (\tilde{T}_i are the temperatures of the reverse configuration.) The vertical lines are the real part of the frequencies of the dissipative normal modes of the system [8]. The areas are proportional to the particle kinetic energies (or temperatures). The rectification coefficient is $R \approx 0.8$: in the forward configuration, the spectra match well while in the reverse configuration there is a clear mismatching.

on the product of the spectra,

$$M = \int F[S_L(\omega)S_R(\omega); \omega] d\omega. \quad (28)$$

The following discussion will find a natural, simple choice for the function F .

We need to average over realizations of the noise. First, we define $X_{Rj}(\omega)$ and $X_{Lj}(\omega)$ as the Fourier transforms of the displacements, $q_{Lj}(t)$ and $q_{Rj}(t)$ respectively, in the j -th realization. We separate real and imaginary parts,

$$\begin{aligned} X_{Rj}(\omega) &= a_j + b_j i, \\ X_{Lj}(\omega) &= c_j + d_j i. \end{aligned} \quad (29)$$

Notice that $X_{Lj}(-\omega) = c_j - d_j i$ because the displacements are real. Therefore,

$$\langle X_R(\omega)X_L(-\omega) \rangle = \sum_j \frac{a_j c_j + b_j d_j + i(c_j b_j - a_j d_j)}{N}, \quad (30)$$

where N is the number of realizations which is supposed to be very large. We are only interested in the imaginary part of (30) according to the flux expression (19). The square of the imaginary part is

$$\begin{aligned} (c_j b_j - a_j d_j)^2 &= a_j^2 d_j^2 + b_j^2 c_j^2 - 2a_j c_j b_j d_j \\ &\leq a_j^2 c_j^2 + b_j^2 d_j^2 + b_j^2 c_j^2 + a_j^2 d_j^2 = (a_j^2 + b_j^2)(c_j^2 + d_j^2). \end{aligned} \quad (31)$$

From this inequality we conclude that

$$|(c_j b_j - a_j d_j)| \leq \sqrt{a_j^2 + b_j^2} \sqrt{c_j^2 + d_j^2}. \quad (32)$$

The absolute value of the imaginary part of the correlation function in Eq. (30) is

$$|\text{Im}[\langle X_R(\omega) X_L(-\omega) \rangle]| = \left| \sum_j^N \frac{c_j b_j - a_j d_j}{N} \right| \quad (33)$$

and, from Eq. (32), it obeys

$$\left| \sum_j^N \frac{c_j b_j - a_j d_j}{N} \right| \leq \sum_j^N \frac{\sqrt{a_j^2 + b_j^2} \sqrt{c_j^2 + d_j^2}}{N}. \quad (34)$$

Now, we apply the Cauchy-Bunyakovsky-Schwarz inequality,

$$\left(\sum_{j=1}^n \alpha_j \beta_j \right)^2 \leq \left(\sum_{j=1}^n \alpha_j^2 \right) \left(\sum_{j=1}^n \beta_j^2 \right), \quad (35)$$

to the right-hand side of (34), with $\sqrt{a_j^2 + b_j^2} = \alpha_j$ and $\sqrt{c_j^2 + d_j^2} = \beta_j$, to find

$$\begin{aligned} \sum_j^N \frac{\sqrt{a_j^2 + b_j^2} \sqrt{c_j^2 + d_j^2}}{N} &\leq \\ \frac{1}{N} \sqrt{\left(\sum_j^N a_j^2 + b_j^2 \right) \left(\sum_j^N c_j^2 + d_j^2 \right)}. \end{aligned} \quad (36)$$

As

$$\begin{aligned} \langle X_R(\omega) X_R(-\omega) \rangle &= \frac{1}{N} \sum_j^N (a_j^2 + b_j^2), \\ \langle X_L(\omega) X_L(-\omega) \rangle &= \frac{1}{N} \sum_j^N (c_j^2 + d_j^2), \end{aligned} \quad (37)$$

we find from Eq. (36) the following inequality for the integrand in Eq. (19),

$$\begin{aligned} &|\text{Im}[\langle X_R(\omega) X_L(-\omega) \rangle]| \\ &\leq \sqrt{\langle X_L(\omega) X_L(-\omega) \rangle \langle X_R(\omega) X_R(-\omega) \rangle}. \end{aligned} \quad (38)$$

Since $\langle X_i(\omega) X_i(-\omega) \rangle$ is related to $S_i(\omega) = \langle W_i(\omega) W_i(-\omega) \rangle$ by Eq. (12), expression (38) can be written as

$$\omega^2 |\text{Im}[\langle X_R(\omega) X_L(-\omega) \rangle]| \leq \sqrt{S_L(\omega) S_R(\omega)}, \quad (39)$$

or using Eq. (19), and taking into account that $|\int f(x) dx| \leq \int |f(x)| dx$,

$$|J| \leq \frac{k}{2\pi} \int \frac{1}{|\omega|} \sqrt{S_L(\omega) S_R(\omega)} d\omega, \quad (40)$$

which sets an upper limit for the heat flux. This relation prompts us to define the function F in Eq. (28) and the matching as

$$M = \frac{k}{2\pi} \int \frac{1}{|\omega|} \sqrt{S_L(\omega) S_R(\omega)} d\omega. \quad (41)$$

This measure of the matching (41) allows for direct comparison between J and M since they have the same dimensions while with other proposed definitions we can only compare their ratios [2]. When so defined, the spectral density matching sets an upper bound for the flux, $|J| \leq M$.

In [21] Li *et al.*, to quantify the overlap between the power spectra between left and right segments, introduced

$$S = \frac{\int_0^\infty S_L(\omega) S_R(\omega) d\omega}{\int_0^\infty S_L(\omega) d\omega \int_0^\infty S_R(\omega) d\omega}. \quad (42)$$

and demonstrated the correlation between the heat fluxes and the overlaps of the spectra. They found numerically the relation $|J/\tilde{J}|^\delta \sim (S/\tilde{S})$, with $\delta = 1.62 \pm 0.10$, in their model, two weakly linearly coupled, dissimilar anharmonic segments, exemplified by a Frenkel-Kontorova chain segment and a neighboring Fermi-Pasta-Ulam chain segment.

Next, we will evaluate the flux and the matching for different parameter configurations for the two-ion model to test the inequality $|J| \leq M$ and also to look for a similar relation to the one found by Li *et al.* but for the matching expression introduced here.

IV. FLUX AND MATCHING FOR THE TWO-ION MODEL

We compute the heat flux and the matching (41) for the two-ion model solving Eqs. (23) and (7) for different parameter configurations. We will only consider the maximal rectification region given by the condition (25).

In Fig. 5 the flux and the matching are displayed as a function of $C = g = a$. As predicted by Eq. (40) the matching is above the flux. Both quantities behave similarly and the difference tends to a constant as C increases. Also, R tends to one, as seen in Fig. 3. The forward and reverse configurations show very different

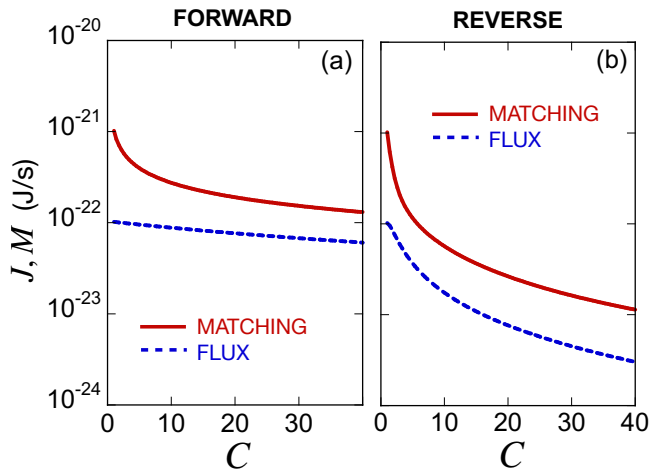


FIG. 5: Flux and matching versus $C = a = g$. $T_L = 1$ mK, $T_R = 0.1$ mK. Other parameters, as explained in the Sec. II C.

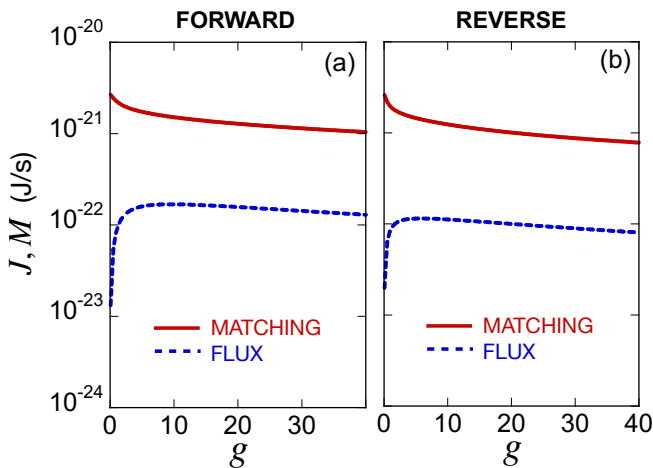


FIG. 6: Flux and matching versus g with a constant mass ratio a . $T_L = 1$ mK, $T_R = 0.1$ mK. Other parameters, as explained in the Sec. II C.

curves (a sign of rectification) as we are following the line of fastest growth of R .

Since experimentally it is not feasible to have a continuum for the masses ratio a , in Fig. 6 we have also plotted J and M fixing the masses for Ca^+ and Mg^+ ions, and sweeping over g . Both quantities behave similarly, except in the region for very low g , but this region is not really interesting since it corresponds to a very low R . Forward and reverse curves are now closer to each other, corresponding to a smaller R , see again Fig. 3.

The flux ratio J/\tilde{J} is exactly linear with C according to Eq. (24), see Fig. 7, whereas the ratio M/\tilde{M} is also linear in C , except for very low C , with a proportionality factor that depends on the ratio of the bath temperatures.

Thus, sweeping over $C = a = g$ a very simple linear relation is found numerically between the ratios J/\tilde{J} and

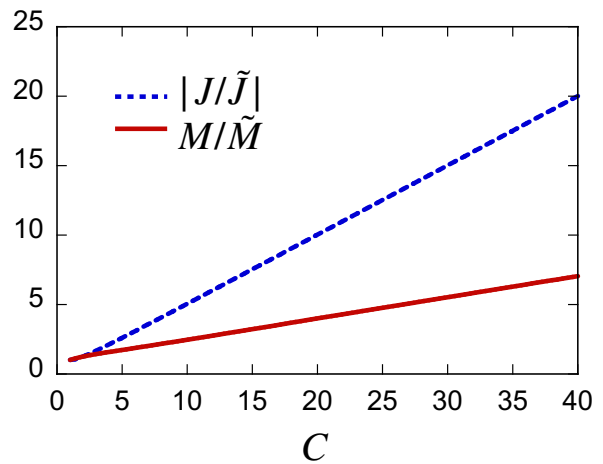


FIG. 7: Forward to reverse ratios J/\tilde{J} and M/\tilde{M} versus C . $T_L = 1$ mK, $T_R = 0.1$ mK

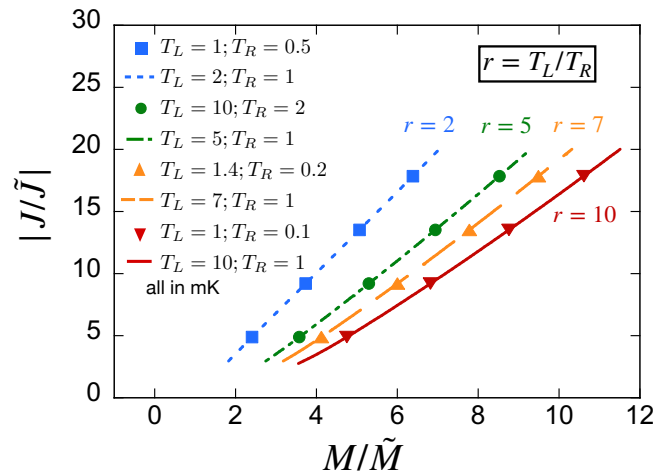


FIG. 8: Flux ratio J/\tilde{J} vs. the matching ratio M/\tilde{M} for different temperature intervals. The line points depend parametrically on C . The slope depends on the ratio of temperatures T_L/T_R . Dots and lines of the same color indicate same temperatures' ratio but different values of the temperatures (in mK) as indicated in the legend. For instance, blue dots correspond to $T_L = 1$ mK and $T_R = 0.5$ mK and the blue line to $T_L = 2$ mK and $T_R = 1$ mK, both cases verify $T_L/T_R = 2$.

M/\tilde{M} for our model,

$$|J/\tilde{J}| \sim M/\tilde{M}, \quad (43)$$

with a proportionality factor that depends on the ratio between temperatures T_L/T_R , as shown in Fig. 8.

V. DISCUSSION

Using a simple, but experimentally feasible model of two ions interacting with laser-induced heat baths, we have defined the power spectrum overlap or “spectral matching” of the ions so that it provides an upper bound

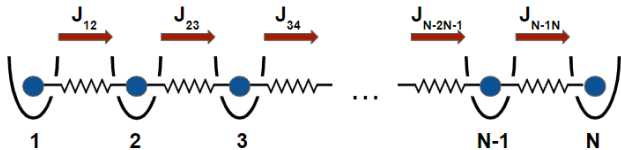


FIG. 9: N -particle linear chain with interaction between nearest neighbors.

to the flux. In fact forward to reverse flux ratios are proportional to matching ratios for the parameter conditions where rectification is optimal. These findings put on a sounder basis the relation between heat rectification and the spectral match or mismatch for forward and reverse bath temperatures.

The results can be generalized to any N -particle chain with linear interactions between nearest neighbors and two thermal baths at the boundaries. The trap potentials could be anharmonic. For the N -particle chain in the steady state $\langle \dot{H}_i \rangle = 0$, see Fig. 9, where H_i is the local energy for the i th particle. Thus the energy flux from particle $i - 1$ to particle i equals the flux from particle i to particle $i + 1$, namely $J_{i-1,i} = J_{i,i+1}$.

The flux that crosses the chain J is

$$J = J_{i,i+1} \quad (44)$$

where i can be $1, 2, 3, \dots, N - 1$. The equations from (13) to (19) and the arguments in Sec. III for ions L and R are valid as well for particles i and $i + 1$, so

$$|J_{i,i+1}| \leq M_{i,i+1}, \quad (45)$$

where $M_{i,i+1}$ is the matching (41) between the spectral densities of ions i and $i + 1$. Therefore

$$|J| \leq M_{i,i+1}, \quad (46)$$

where i can be $1, 2, 3, \dots, N - 1$. Eq. (46) is the generalization of our results for an N -particle linear chain and it states that the flux through the chain is bounded by the spectral matching of nearest-neighbor particles.

Acknowledgments

We thank Miguel Ángel Simón for useful discussions. We thank the Grant PID2021-126273NB-I00 funded by MCIN/AEI/ 10.13039/501100011033 and by “ERDF A way of making Europe”. We acknowledge financial support from the Basque Government Grant No. IT1470-22. MP acknowledges support from the Spanish Agencia Estatal de Investigación, Grant No. PID2019- 107609GB-I00.

-
- [1] N. Roberts and D. Walker, *International Journal of Thermal Sciences* **50**, 648 (2011), ISSN 1290-0729.
 - [2] N. Li, J. Ren, L. Wang, G. Zhang, P. Hänggi, and B. Li, *Rev. Mod. Phys.* **84**, 1045 (2012).
 - [3] E. Pereira, *EPL (Europhysics Letters)* **126**, 14001 (2019).
 - [4] L. Wang and B. Li, *Phys. Rev. Lett.* **99**, 177208 (2007).
 - [5] B. Li, L. Wang, and G. Casati, *Appl. Phys. Lett.* **88**, 143501 (2006).
 - [6] T. Ma and Y. Wang, in *Carbon Based Nanomaterials for Advanced Thermal and Electrochemical Energy Storage and Conversion*, edited by R. Paul, V. Etacheri, Y. Wang, and C.-T. Lin (Elsevier, 2019), *Micro and Nano Technologies*, pp. 103 – 119, ISBN 978-0-12-814083-3.
 - [7] M. A. Simón, S. Martínez-Garaot, M. Pons, and J. G. Muga, *Phys. Rev. E* **100**, 032109 (2019).
 - [8] M. A. Simón, A. Alaña, M. Pons, A. Ruiz-García, and J. G. Muga, *Phys. Rev. E* **103**, 012134 (2021).
 - [9] C. Starr, *Physics* **7**, 15 (1936).
 - [10] S. Chen, E. Pereira, and G. Casati, *Europhysics Letters* **111**, 30004 (2015).
 - [11] J. Moon and R. Normes Keeler, *International Journal of Heat and Mass Transfer* **5** **89**, 967971 (1962).
 - [12] C. Marucha, J. Mucha, and J. Rafałowicz, *Physica Status Solidi A* (1976).
 - [13] M. Alaghemandi, E. Algaer, M. C. Böhm, and F. Müller-Plathe, *Nanotechnology* **20**, 115704 (2009).
 - [14] M. Terraneo, M. Peyrard, and G. Casati, *Phys. Rev. Lett.* **88**, 094302 (2002).
 - [15] L. Defaveri and C. Anteneodo, *Phys. Rev. E* **104**, 014106 (2021).
 - [16] J. Wang, E. Pereira, and G. Casati, *Phys. Rev. E* **86**, 010101 (2012).
 - [17] E. Pereira and R. R. Ávila, *Phys. Rev. E* **88**, 032139 (2013).
 - [18] M. Pons, Y. Y. Cui, A. Ruschhaupt, M. A. Simón, and J. G. Muga, *EPL (Europhysics Letters)* **119**, 64001 (2017).
 - [19] T. J. Alexra, *Phys. Rev. E* **101**, 062122 (2020).
 - [20] J.-P. Eckmann and C. Mejía-Monasterio, *Phys. Rev. Lett.* **97**, 094301 (2006).
 - [21] B. Li, J. Lan, and L. Wang, *Phys. Rev. Lett.* **95**, 104302 (2005).
 - [22] B. Li, L. Wang, and G. Casati, *Phys. Rev. Lett.* **93**, 184301 (2004).
 - [23] E. Pereira, *Phys. Rev. E* **96**, 012114 (2017).
 - [24] A. Ruiz-García, J. J. Fernández, and D. Alonso, *Phys. Rev. E* **99**, 062105 (2019).
 - [25] A. Ruiz, D. Alonso, M. B. Plenio, and A. del Campo, *Phys. Rev. B* **89**, 214305 (2014).
 - [26] T. Pruttivarasin, M. Ramm, I. Talukdar, A. Kreuter, and H. Häffner, *New Journal of Physics* **13**, 075012 (2011).
 - [27] N. Freitas, E. A. Martinez, and J. P. Paz, *Physica Scripta* **91**, 013007 (2015).
 - [28] C. D. Bruzewicz, J. Chiaverini, R. McConnell, and J. M.

Sage, Applied Physics Reviews **6**, 021314 (2019).

[29] S. Särkkä and A. Solin, *Applied Stochastic Differential*

Equations (Cambridge University Press, 2019).